

Journal of Biomedical Optics

SPIEDigitalLibrary.org/jbo

Dual-wavelength polarimetric glucose sensing in the presence of birefringence and motion artifact using anterior chamber of the eye phantoms

Bilal H. Malik
Casey W. Pirnstill
Gerard L. Coté

Dual-wavelength polarimetric glucose sensing in the presence of birefringence and motion artifact using anterior chamber of the eye phantoms

Bilal H. Malik, Casey W. Pirnstill, and Gerard L. Coté

Texas A&M University, Department of Biomedical Engineering, 5045 Emerging Technologies Building, 3120 TAMU, College Station, Texas

Abstract. Noninvasive glucose monitoring is being investigated as a tool for effectively managing diabetes mellitus. Optical polarimetry has emerged as one such method, which can potentially be used to ascertain blood glucose levels by measuring the aqueous humor glucose levels in the anterior chamber of the eye. The key limitation for realizing this technique is the presence of sample noise due to corneal birefringence, which in the presence of motion artifact can confound the glucose signature in the aqueous humor of the eye. We present the development and characterization of a real-time, closed-loop, dual-wavelength polarimetric system for glucose monitoring using both a custom-built plastic eye phantom (*in vitro*) and isolated rabbit corneas (*ex vivo*) mounted in an artificial anterior chamber. The results show that the system can account for these noise sources and can monitor physiologic glucose levels accurately for a limited range of motion-induced birefringence. Using the dual-wavelength system *in vitro* and *ex vivo*, standard errors were 14.5 mg/dL and 22.4 mg/dL, respectively, in the presence of birefringence with motion. The results indicate that although dual-wavelength polarimetry has a limited range of compensation for motion-induced birefringence, when aligned correctly, it can minimize the effect of time-varying corneal birefringence for a range of motion larger than what has been reported *in vivo*. © 2013 Society of Photo-Optical Instrumentation Engineers (SPIE). [DOI: 10.1117/1.JBO.18.1.017007]

Keywords: diabetes; glucose sensing; corneal birefringence; optical polarimetry; eye phantom.

Paper 12181 received Mar. 16, 2012; revised manuscript received Oct. 21, 2012; accepted for publication Dec. 13, 2012; published online Jan. 8, 2013.

1 Introduction

Our group has proposed optical polarimetry through the anterior chamber of the eye for noninvasive monitoring of glucose, which can potentially serve as a tool to improve the management of diabetes.¹ One of the main challenges with using polarimetry for glucose sensing *in vivo* is that most of the biological tissues are optically turbid. Polarimetric sensing of glucose in such media thus becomes challenging due to the presence of relatively high concentrations of chiral components, such as albumin, and multiple scattering events, which can significantly confound the state of polarization of the reflected or transmitted light.² Thus, one possible way to overcome these problems is by propagating polarized light through the anterior chamber of the eye, including the cornea and aqueous humor (AH), where the absorption and scattering effects are minimal and glucose is the principal chiral component.³

The cornea, in particular, not only serves as the gateway into the eye for vision, but also for potential optical monitoring of analytes such as glucose. It is the major refractive structure along with the ocular lens, focusing light onto the retina. The fibrous collagen of the cornea is responsible for its mechanical strength and aids in maintaining the ocular contour; in addition, it is a source of optical birefringence.⁴ These collagen fibers are primarily present in the stromal region, which constitutes more than 90% of the cornea. The regular arrangement and uniformity of these fibers plays a major role in maintaining corneal

transparency.⁵ Any disturbance in such an arrangement can result in significant scattering of the transmitted light and, therefore, adversely impact optical clarity of the cornea.⁶

As mentioned, the fibrous structure of the stroma makes the cornea birefringent, which varies spatially across the surface of the cornea.⁷⁻⁹ Birefringence in structured materials such as linear retarders is characterized by $\Delta n = (n_e - n_o)$, which is the difference between the extraordinary and ordinary refractive indices (i.e., n_e and n_o , respectively).¹⁰ In the case of the cornea, individual constituent collagen fibrils can be regarded as linear retarders with the direction of the fast axis oriented perpendicular to the fibril orientation.¹¹ When such birefringent layers are arranged on top of each other with different orientations of their fast axes, the overall composition exhibits a type of birefringence known as form birefringence.¹² Several models have been proposed to explain this behavior of corneal birefringence.^{7,8,13-18} Most of these models agree that birefringence is at its minimum at the center of the cornea and increases monotonically toward the peripheral regions of the cornea. These models also indicate that the effective birefringence increases as the angle of incidence with respect to the surface normal of the cornea increases.

One of the difficulties associated with polarimetric glucose monitoring through the eye is the corneal birefringence coupled with motion artifact. This time-varying birefringence is the most significant source of noise when attempting polarimetric glucose sensing in the anterior chamber of the eye, wherein it confounds the signature of the optical activity of glucose by contributing a significant change in the state of

Address all correspondence to: Bilal H. Malik, Texas A&M University, Department of Biomedical Engineering, 5045 Emerging Technologies Building, 3120 TAMU, College Station, Texas. Tel: 979-458-2322; Fax: 979-845-4450; E-mail: malik@tamu.edu

polarization of the probing light.⁹ Our group has quantified the effect of corneal birefringence on glucose sensing through the eye both theoretically and experimentally.¹⁹ Although a simplified model was used in this previous work, it was clear from the research that time-varying corneal birefringence is a significant source of noise in the system. It is, therefore, important to account for time-varying corneal birefringence due to motion artifacts in order to predict accurately the glucose concentration in the AH of the eye.

To date, the two mechanisms that are being researched to address the noise due to time-varying corneal birefringence in polarimetric glucose monitoring are the use of a dedicated birefringence compensator and a dual-wavelength polarimeter.^{1,20,21} Specifically, Cameron and Anumula utilized a dedicated birefringence compensator to attempt to account for corneal birefringence.²⁰ Their system includes a variable retarder that has the potential to compensate for birefringence by negating the contribution of sample birefringence. Our group has utilized dual-wavelength polarimetry, which effectively uses two wavelengths to build a multiple linear regression (MLR) model to minimize the contribution of motion-induced birefringence to the total rotation of the state of polarization, yet remains sensitive to a change in rotation due to glucose.^{1,21} This reduction in the effect of time-varying corneal birefringence is limited to a narrow but significant range of birefringence values.

Other embodiments of polarimetric glucose sensing through the eye include reflection of light from the intraocular lens (IOL). Rawer et al. utilized an open-loop system to measure the rotation of plane of polarization of light by glucose in the AH of the eye.²² The eye phantom used an artificial cornea and an artificial IOL to enhance the reflectance at the AH-IOL interface, which otherwise is lower than 0.5%. The system was tested in the glucose concentration range of 0 to 40 g/dL, with the smallest glucose concentration at 10 g/dL, more than 1000 times the physiological range. Although the authors discuss the effect that eye movements can have on the system, they conclude that further system optimization is needed to allow for high-speed compensation of eye motion. A similar but more advanced system was proposed by Ansari et al., which exploited the reflection at AH-IOL interface at Brewster's angle, wherein a plano-convex lens was used as an artificial IOL, but this too does not have the ability to overcome changes in the signal due

to motion artifacts.²³ More recently, Purvinis et al. used an open-loop, single-wavelength polarimeter to measure the glucose concentration in the eye *in vivo*.²⁴ Therein, the motion artifacts were reduced and effectively eliminated by limiting animal motion, and the authors concluded that corneal birefringence compensation, along with closed-loop control, can provide more robust measurements.

In this article, we focus on overcoming the realistic motion artifact seen *in vivo* by measuring physiological glucose concentrations in a moving plastic eye model (*in vitro*) and moving New Zealand White rabbits' corneas mounted in a pressurized artificial anterior chamber (*ex vivo*) using a custom-built, near-real-time, dual-wavelength, polarimetric glucose sensing system. The description of the dual-wavelength polarimetric system and the unique eye phantoms along with the results are described here.

2 Theory

2.1 Optical System

Let us consider the whole optical train from the light source to the photodetector, as depicted in Fig. 1. The equation for the electric field at the detector can be derived using the Jones vector calculus.²⁵ For a given wavelength, the optical system can be modeled as a linear polarizer, followed by two Faraday rotators (compensator and modulator), the eye model, and finally the analyzer. When the initial polarizer is aligned with either the fast or the slow axis, the resulting system matrix representation is

$$\begin{aligned}
 V_{\text{system}} = & \begin{pmatrix} 1 & 0 \\ 0 & 0 \end{pmatrix} \begin{matrix} \text{Eye Model} \\ \left[\begin{array}{cc} \cos(\phi_g) e^{-i\frac{\delta_1(t)+\delta_2(t)}{2}} & \sin(\phi_g) e^{-i\frac{\Delta\delta(t)}{2}} \\ -\sin(\phi_g) e^{-i\frac{\Delta\delta(t)}{2}} & \cos(\phi_g) e^{i\frac{\delta_1(t)+\delta_2(t)}{2}} \end{array} \right] \end{matrix} \\
 & \times \left\{ \begin{matrix} \text{Faraday Modulator} \\ \left[\begin{array}{cc} \cos[\theta_m \sin(\omega_m t)] & -\sin[\theta_m \sin(\omega_m t)] \\ \sin[\theta_m \sin(\omega_m t)] & \cos[\theta_m \sin(\omega_m t)] \end{array} \right] \end{matrix} \right\} \\
 & \times \begin{matrix} \text{Faraday Compensator} & \text{Polarizer} \\ \left[\begin{array}{cc} \cos(\phi_f) & \sin(\phi_f) \\ -\sin(\phi_f) & \cos(\phi_f) \end{array} \right] \begin{pmatrix} 0 & 0 \\ 0 & 1 \end{pmatrix} \end{matrix}, \quad (1)
 \end{aligned}$$

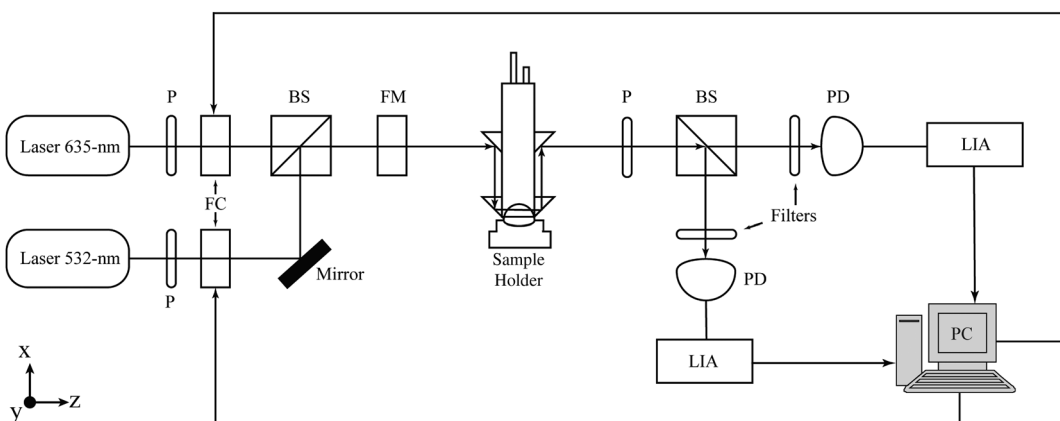


Fig. 1 Experimental setup of the dual-wavelength optical polarimeter. Note that the sample holder can either be the plastic ocular phantom (for *in vitro* experiments) or the artificial anterior chamber phantom (for fixing isolated corneas). The two ports on the top of the eye coupling device are used to fill in the tube with PBS solution in order to accomplish index matching. P, polarizer; FC, Faraday compensator; BS, beam-splitter; FM, Faraday modulator; PD, photodetector; LIA, lock-in amplifiers.

where V_{system} is the system-equivalent Jones matrix; ϕ_g and ϕ_f represent changes in optical rotation due to glucose and optical rotation from the Faraday compensator, respectively; $\delta_1(t)$ and $\delta_2(t)$ are the amount of retardation from entering and exiting the cornea as a function of time; $\Delta\delta(t) = \delta_1(t) - \delta_2(t)$ is the difference between them; θ_m is the modulation depth for the Faraday modulator; and ω_m is the modulation frequency.

$$\text{Linear Retarder}[\Delta nL(t), \theta, \lambda] = \left\{ \begin{array}{cc} \cos\left[\frac{\pi}{\lambda} \Delta nL(t)\right] - i \cos(2\theta) \sin\left[\frac{\pi}{\lambda} \Delta nL(t)\right] & -i \sin(2\theta) \sin\left[\frac{\pi}{\lambda} \Delta nL(t)\right] \\ -i \sin(2\theta) \sin\left[\frac{\pi}{\lambda} \Delta nL(t)\right] & \cos\left[\frac{\pi}{\lambda} \Delta nL(t)\right] + i \cos(2\theta) \sin\left[\frac{\pi}{\lambda} \Delta nL(t)\right] \end{array} \right\}, \quad (2)$$

where θ represents the orientation of the slow axis with respect to the system's x -axis, λ is the wavelength of light, and ΔnL is the amount of linear retardance in units of length. The optical rotator element can be represented as

$$\text{Optical Rotator}(\phi_g) = \begin{bmatrix} \cos(\phi_g) & \sin(\phi_g) \\ -\sin(\phi_g) & \cos(\phi_g) \end{bmatrix}. \quad (3)$$

The resulting overall eye model matrix would vary with respect to both the azimuth angle and the ellipticity of the state of polarization. Further, the ellipticity is affected primarily by the retardation, where the time-varying retardation $\delta(t)$ introduced due to the cornea is given in Eq. (2) by

$$\delta(t) = \frac{2\pi}{\lambda} \Delta nL(t), \quad (4)$$

where λ is the wavelength, $\Delta n = |n_e - n_o|$ is the corneal birefringence, and $L(t)$ is the path length through the cornea, which varies as a function of time.

$$\text{Linear Retarder}[\delta_2(t)] \text{Optical Rotator}(\phi_g) \text{Linear Retarder}[\delta_1(t)] = \begin{bmatrix} \cos(\phi_g) e^{-i\frac{\delta_1(t)+\delta_2(t)}{2}} & \sin(\phi_g) e^{i\frac{\Delta\delta(t)}{2}} \\ -\sin(\phi_g) e^{-i\frac{\Delta\delta(t)}{2}} & \cos(\phi_g) e^{i\frac{\delta_1(t)+\delta_2(t)}{2}} \end{bmatrix}, \quad (5)$$

where, as stated above, $\delta_1(t)$ and $\delta_2(t)$ are the amount of retardation from entering and exiting the cornea, $\Delta\delta(t)$ is the difference between $\delta_1(t)$ and $\delta_2(t)$, and ϕ_g is the optical rotation caused by the glucose within the aqueous humor.

The primary relationship in overall system voltage, shown in Eq. (1), that contributes to the net optical rotation is the matrix that represents the eye model. The net optical rotation from this matrix can be isolated from a generalized retarder Jones matrix, as pointed out by Winkler et al.,²⁶ using a Jones matrix decomposition as shown by Savenkov et al.²⁷ Using a combination of Eq. (5) and the Jones matrix decomposition described by Savenkov et al., the net optical rotation in the eye can be calculated from the following equation.^{26,27}

$$\tan(\phi_{\text{net}}) = \tan(\phi_g) \times \frac{\cos\left[\frac{\Delta\delta(t)}{2}\right]}{\cos\left[\frac{\delta_1(t)+\delta_2(t)}{2}\right]}. \quad (6)$$

It has been shown by Winkler et al., that the eye can be represented as a series of diattenuators, linear retarders, and an optical rotator.²⁶ If index matching is used for coupling the light through the eye, the Jones matrices for anterior and posterior diattenuation can drop out of the eye model. Thus, according to the Winkler model,²⁶ the Jones matrix of the eye phantom shown in Eq. (1) is presented as an optical rotator between two linear retarders.²⁶ A linear retarder is of the following form:

The corneal birefringence at the entrance and exit beam path has an effect on the perceived optical rotation. This effect can be illustrated through Jones matrix decomposition and the Jones calculus. In the collected data from the eye models presented in the results and discussion section of this article, the initial polarizers and the analyzer were adjusted for each wavelength at the beginning of each test run to allow for compensation voltages to nullify the system. The direct consequence of this adjustment is that the effects of corneal birefringence were minimized through alignment of the linear polarization vector near the slow axis of the cornea. Specifically, for both eye models presented, the net perceived optical rotation due to both birefringence and glucose remained under a limit of rotation of ± 1 deg, the maximum modulation depth of the faraday modulator, in order for the compensation device to provide adequate feedback to nullify the system. Thus, as depicted in Eq. (1) for the eye model and consistent with the Winkler model,²⁶ when the fast axis or slow axis of a linear retarder (cornea) is aligned along the x -axis (of Fig. 1), a simplified Jones matrix representing the eye can be shown as the product of two linear retarders and an optical rotator:²⁶

This equation can be further simplified because the optical rotation caused by glucose concentration in the physiologic range is very small. Thus, the tangent of this angle is very close to the actual angle in radians. Additionally, equal retardation on both corneal surfaces was assumed in the model; however, this assumption is not a physical requirement for the experimental system to work. When this occurs, the term $\cos[\Delta\delta(t)/2]$ becomes approximately equal to 1 and $\delta(t) = [\delta_1(t) + \delta_2(t)]/2$. Thus, Eq. (6) can be simplified as

$$\tan[\phi_{\text{net}}(\lambda)] = \phi_g \times \frac{1}{\cos[\delta(t)]} = \frac{\phi_g}{\cos\left[\frac{2\pi}{\lambda} \Delta nL(t)\right]}. \quad (7)$$

As indicated in our previous publications,¹ MLR analysis was used to accommodate the contribution of birefringence. The respective data points (voltages input into the Faraday compensators) for both wavelengths, along with the known concentrations, were used to calculate optimal weights, which then serve

as coefficients for the construction of the MLR model. Specifically, the single-wavelength models were of the form $[C_g] = a.V + a_0$, where $[C_g]$ is the glucose concentration, V is the corresponding voltage signal applied to the Faraday compensator used to null the detected signal via a closed-loop proportional-integral-derivative (PID) controller, and a_1 and a_0 are calibration coefficients. The general case for the dual-wavelength model generated by MLR analysis was of the form²⁸

$$[C_g] = a_1 V_{\lambda 1} + a_2 V_{\lambda 2} + a_0, \quad (8)$$

where $V_{\lambda 1}$ and $V_{\lambda 2}$ are voltage signals applied to the Faraday compensators by the PID controller to nullify the system for the corresponding two single-wavelength models, and a_1 , a_2 , and a_0 are calibration coefficients that serve as weights for the scaled regression model.

The best values for the coefficients were determined by setting up the sum of the squares of the residuals and differentiating with respect to each of the unknown coefficients.²⁸ The coefficients yielding the minimum sum of the squares residuals can be obtained by the following matrix relationship:

$$\begin{pmatrix} a_0 \\ a_1 \\ a_2 \end{pmatrix} = [(P)^T(P)]^{-1} [P]^T[C_g] = [Q][C_g], \quad (9)$$

where $[Q]$ is calculated using basic mathematical combinations of the matrices shown above.²⁸ The matrix $[P]^T$ was obtained by transposing the matrix $[P]$, which is calculated by solving a set of simultaneous linear equations.²⁸ It should be noted that the matrix $[P]$ in Eq. (9) was formed from the system compensation voltages and had elements with dimensions (n by $p + 1$), where p is the number of coefficients, or number of wavelength voltages utilized plus 1; and n is the number of signals used. Thus, the resulting matrix $[P]$ for the dual-wavelength setup had dimensions of two by three elements and the response vector, $[C_g]$, was a 2-D vector. Note that $[P]$ is commonly referred to as the design matrix in a multiple linear regression analysis and contains the system voltage information in the dual-wavelength model. A more rigorous treatment of MLR can be found in Ref. 28. Using MLR allows for minimization of the noise due to linear changes in birefringence induced with motion for small values of birefringence, as discussed in the Sec. 3 later in this article. With the noise minimized using the dual-wavelength approach, accurate monitoring of optical activity due to glucose can be calculated in the presence of this limited, but significant, time-varying corneal birefringence.

It is known, as shown in Eq. (4), that the optical retardation for a birefringent sample is a function of both the wavelength and the birefringence $|n_e - n_o|$ for a fixed path length through the cornea. In the case of the cornea, the birefringence quantity $|n_e - n_o|$ is known to be constant with wavelength at a particular location, a behavior attributed to the *form* birefringence of the cornea.^{8,29,30} Also, for a given point in space and time, t_0 , (i.e., with no motion), Δn and $L(t_0)$ are constant, and the product of $1/\lambda$ and these values is fixed. Therefore, for a given time, the retardance values, $\delta_{\lambda 1}(t)$ and $\delta_{\lambda 2}(t)$, can be minimized using MLR, so long as the wavelengths are known (635 and 532 nm in this case) because the values change in a scaled linear fashion with respect to path length $L(t)$. Further, because the compensation voltage V_λ is the voltage required to nullify the net optical rotation, it is approximately equal to the tangent of the net optical rotation calculated using Eq. (7). Thus, from the

relationships shown above between the variables associated with optical rotation and wavelength, MLR can be used to extract the glucose concentration at two wavelengths, as shown here:

$$\begin{aligned} \text{MLR}_{\text{signal}} &= a_0 + a_1 V_{\lambda 1} + a_2 V_{\lambda 2} \\ &= a_0 + a_1 \left\{ \frac{\phi_{g\lambda 1}}{\cos \left[\frac{2\pi}{\lambda_1} \Delta n L(t) \right]} \right\} \\ &\quad + a_2 \left\{ \frac{\phi_{g\lambda 2}}{\cos \left[\frac{2\pi}{\lambda_2} \Delta n L(t) \right]} \right\}, \end{aligned} \quad (10)$$

where a_0 is the intercept coefficient generated by MLR fitting and $\phi_{g\lambda_i} = [\alpha]_{\lambda_i}^T [C_g]$.

2.2 Eye Model Parameters

In our system, we utilized the eye model described in detail previously.^{9,19} The input beam diameter was fixed at 1 mm. The values used for n_o and n_e are 1.3760 and 1.3744 (i.e., $|\Delta n| = 1.6 \times 10^{-3}$).

It has been shown that the effect of motion artifacts is minimized in the region near the midpoint between the corneal apex and limbus (i.e., 1.5 mm below the apex).⁹ Therefore, this point was chosen as the center point in the range of motion. The beam position was then changed from 1.48 to 1.52 mm below the apex at frequency of ~ 3 Hz.

3 Materials and Methods

3.1 Dual-Wavelength Optical Polarimeter

The optical setup is illustrated in Fig. 1. The two optical sources included a 635-nm-wavelength laser diode module (Power Technology, Inc., Little Rock, AR) emitting at 7 mW, and a 532-nm wavelength diode-pumped solid-state laser module (Aixiz LLC, Houston, TX) emitting at 10 mW. The output beams, with diameters of approximately 1 mm, from both sources were linearly polarized using Glan-Thompson linear polarizers (Thorlabs, Newport, NJ). The individual beams passed through respective Faraday rotators that operate as rotation compensators in order to achieve closed-loop feedback control. The Faraday rotators were made of Terbium Gallium Garnet (TGG) optical rods wrapped with an inductive solenoid coil. The TGG crystals (Deltronic Crystals Inc., Dover, NJ) had a high Verdet constant to give the desired optical rotation for the field generated. The custom-built coil was driven by current amplifiers to create the field necessary to produce the appropriate optical rotation compensation. A beam-splitter/combiner (Optosigma Corp., Santa Ana, CA) was used to combine and lay the two individual beams on top of each other. The direction of linear polarization was modulated using a Faraday rotator set at 1.09 kHz with a modulation depth of approximately ± 1 degree. The dual light beams were then passed through the unique sample chambers (the plastic eye model or a mounted cornea) as described in detail below. The beam was positioned near the midpoint between the corneal apex and limbus. The sensing path lengths at these positions were calculated to be approximately 8.5 and 6.5 mm for the *ex vivo* and *in vitro* phantoms, respectively. The glucose concentration was varied from 0 to 600 mg/dL in steps of 100-mg/dL.

Note that most commercially available glucose monitors were made to work within this range of glucose concentrations with target accuracy of within 20% of a laboratory standard measurement.^{31,32} The induced motion artifact of the sample was generated using a programmable translation stage (Thorlabs, Newton, NJ). The direction of the induced motion was up and down along the cornea-retina longitudinal axis with the frequency of motion kept at approximately 3 Hz, and the range of motion was fixed at 100 μm for the *in vitro* eye model and 50 μm for the *ex vivo* cornea. These spatial variations were notably higher than what is normally seen *in vivo* in humans in the direction of induced motion, where the range of motion has been cited to be within 15 to 25 μm .³³ For the range of motion used in our experiments, after alignment of the polarizers and analyzer within a sample, the change in the polarization with the slow axis of the eye was found to be small as a function of beam position on the cornea, and more important, within the compensation capabilities of the Faraday compensators. The light then passed through another linear polarizer—an analyzer, which is oriented perpendicular to the initial polarizers. After passing through a beam-splitter, the two wavelengths were then separated using bandpass filters at respective wavelengths (635 and 532 nm). The separate beams were then converted to electronic signals using two PIN photodiodes (Thorlabs, Newton, NJ). The electrical signal from the diodes were amplified using wide-bandwidth amplifiers (CVI Melles Griot, Albuquerque, NM) and sent to lock-in amplifiers (Stanford Research Systems, Sunnyvale, CA) for noise reduction outside the frequency band of interest. The DC signals produced by the lock-in amplifiers served as inputs to a PID controller programmed in LabVIEW 8.9 (National Instruments, Austin, TX). The outputs of this controller then drove the two compensating Faraday rotators through a driver circuit. Each measured output was calculated using a 10-point running average. It should be noted that real-time response of the feedback system is essential in order to overcome the motion artifact. The primary motion-induced corneal birefringence artifact in a rabbit model is mainly due to the respiratory cycle (~ 1.5 Hz) and, to a lesser degree, the cardiac cycle (~ 3.4 Hz).³⁴ As of now, our PID control feedback mechanism takes about 100 ms to reach stability, which is sufficient to overcome motion artifacts due to both respiratory and cardiac cycles. In both of the eye models described below, the initial polarizers and analyzer were adjusted for each wavelength to deliver a minimum signal at the detector during the beginning of each test run, allowing for a low initial compensation voltage to nullify the system. This adjustment minimized the effects of birefringence by relative alignment of the symmetry point of the modulator, and thereby, matched the linear polarization vector of incident light with the effective slow axis of the eye. The dual-wavelength approach utilizing an MLR methodology, as described herein, is capable of compensating for a limited range of change in time-varying corneal birefringence. However, as described above, when the position of the beam is oriented around 1.5 mm below the corneal apex, as performed in the eye model experiments described below, changes in birefringence due to motion can be minimized for a limited range.

3.2 Eye Coupling Mechanism

An in-house-built eye coupling device, shown in Fig. 2, was used to couple light in and out of the anterior chamber of the eye phantom. The device consisted of an inverted glass tube

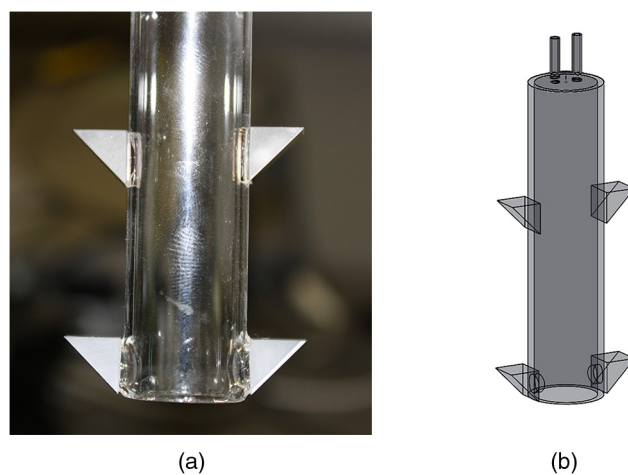


Fig. 2 Photograph (a) and CAD model (b) of the eye coupling device. The glass test tube can be filled with PBS solution to allow for index-matched coupling through the isolated corneas clamped on the artificial anterior chamber phantom.

with four 1-cm reflecting prisms (Thorlabs, Newton, NJ) attached in a periscope configuration. The glass tube was filled with phosphate buffered saline (PBS) solution, which allowed index-matched coupling through the mounted *ex vivo* corneas and resulted in a straight path through the anterior chamber while minimizing beam divergence and deflection.¹ The presence of PBS solution also kept the cornea hydrated and helped reduce epithelium degradation.⁶

3.3 Plastic Eye Model

For *in vitro* operation, a custom-built ocular eye model (Ocular Instrument Inc., Bellevue, WA) was used to mimic the anterior chamber of the eye. As shown in Fig. 3, the anterior chamber of the eye was retrofitted with 0.5 mm infusion tubes. This modification allowed the glucose concentration in the anterior chamber to be changed. The piece mimicking the cornea is made out of poly methyl methacrylate (PMMA) which has a refractive index of 1.489 and a central thickness of 0.55 μm . The value of n_e is not known exactly for the PMMA phantom, however, the literature has shown that the stress dependent birefringence can vary the $|\Delta n|$ within 0.1×10^{-3} to 0.3×10^{-3} .³⁵



Fig. 3 Photograph of the custom-built ocular model. Note that the chamber is fitted with two infusion tubes, which allows changing of glucose concentration in the anterior section.

In our experiments, the PMMA polymer eye phantom was determined to be spatially birefringent (i.e., the birefringence changed as a function of induced motion). The inherent birefringence is mainly caused by the orientation of polymer main chains during injection molding and extrusion processing.³⁵ The change in PMMA birefringence as a function of motion was observed to be three to four times smaller than that of isolated corneas. The relative index mismatch between the refractive indices of PMMA and PBS ($n = 1.33$) did not allow for perfect index-matched coupling using the abovementioned eye coupling device. Instead, the anterior chamber was immersed in a large glass cuvette (Starna Cells, Inc., Atascadero, CA) filled with PBS. The index mismatch resulted in a slight deviation of the beam leaving the anterior chamber relative to the input beam and, therefore, the detection side of the optical system had to be adjusted accordingly. Finally, the eye phantom was mounted on a programmable translation stage to induce motion artifacts.

3.4 Ex Vivo Mounted Corneas

Corneas ($n = 3$) were harvested from New Zealand White rabbits. All corneas were visually inspected and were visibly transparent before, during, and after the *ex vivo* measurements. Excised corneas with 2 to 3 mm of scleral rim were mounted on an artificial anterior chamber (Katena Products, Denville, NJ), as shown in Fig. 4. The base of the chamber comes fitted with two ports to inflate the anterior chamber, which were used to change the glucose concentration in the anterior chamber of the eye. The central thickness of the New Zealand White corneas was approximately $0.4 \mu\text{m}$.³⁶ The corneal birefringence depends on the intraocular pressure within the anterior chamber of the eye. Such behavior and relationship has been studied in detail previously.³⁷ In our experiments, the hydrostatic pressure within the chamber was maintained at the intraocular pressure level of $15 \pm 0.1 \text{ mmHg}$. Similar to the plastic eye phantom, the mount to hold the artificial chamber was fitted on a translation stage to achieve motion artifact.

4 Results and Discussion

The results of the dual-wavelength polarimetric system for determining glucose concentration inside the anterior chamber of the plastic eye phantom are presented in Figs. 5 and 6. The



Fig. 4 Photograph of an isolated cornea clamped on the artificial anterior chamber. Note that the clamping region is within the sclera, which can minimize stress on the cornea.

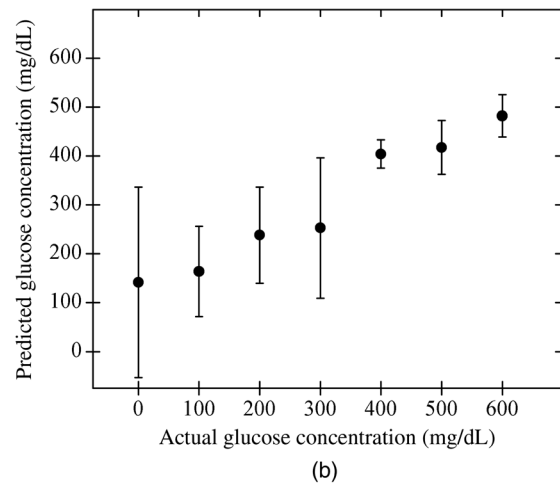
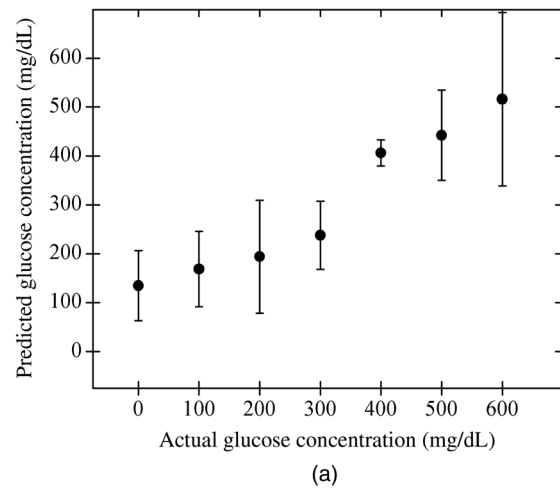


Fig. 5 Mean estimated glucose concentration as a function of actual glucose concentration for the *in vitro*, single-wavelength model using (a) 635-nm and (b) 532-nm wavelengths. Note that the error bars represent the variation between four separate experiments and are large, showing the inability of a single-wavelength model to predict glucose concentration.

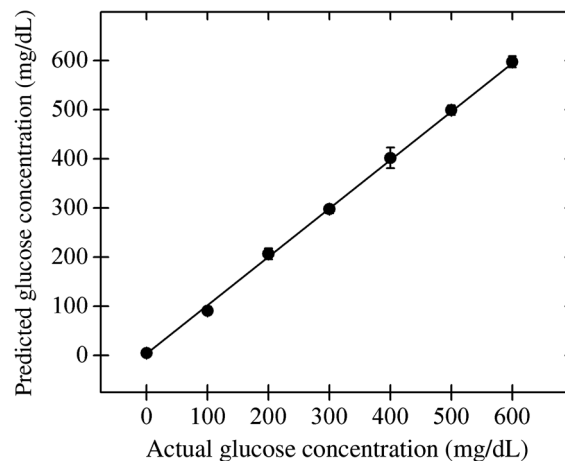


Fig. 6 Mean estimated glucose concentration as a function of actual glucose concentration for the *in vitro*, dual-wavelength model. The error bars represent the variations among four separate experiments and are reduced significantly relative to the single-wavelength models.

experiment was repeated four times across the physiological glucose concentration range of 0 to 600 mg/dL. Figure 5(a) and 5(b) shows the single-wavelength polarimetric measurements for 635-nm and 532-nm wavelengths, respectively. As anticipated, these results indicate that a linear model based on a single wavelength is unable to predict glucose concentration in the presence of motion artifacts. As mentioned earlier, such a system is unable to differentiate between the rotation due to optical activity of glucose and due to the time-varying birefringence. The mean standard error of prediction of glucose concentration is 113.5 mg/dL and 136.5 mg/dL for 635-nm and 532-nm wavelengths, respectively. However, when the measurements from individual single wavelengths are treated with MLR analysis, the effect of birefringence is significantly reduced, as shown in Fig. 6. The dual-wavelength system response is much more linear compared to either of the individual wavelength responses, and the mean standard error of prediction is reduced by an order of magnitude to 14.5 mg/dL, with a correlation coefficient of 0.998. However, in the simulations of Eq. (8), the dual-wavelength MLR method could only be used to compensate for birefringence across a limited, but significant, range of motion that was on the order of what has been reported *in vivo* in humans.³³

Although the application of dual-wavelength polarimetry to *in vitro* glucose sensing in the polymer eye phantom served to demonstrate how this technique can be applied *in vivo*, physiological sample noise conditions due to actual corneal birefringence, as well as the refractive index difference between the cornea (1.376) and the polymer (1.489), are different. Thus, we extended the application of our approach to excised cornea tissue mounted in an artificial anterior chamber. Since our eye coupling mechanism allows the light to travel straight through the anterior chamber, without interacting with any ocular tissues other than the cornea, the mounted excised corneas more closely represent physiological conditions. Although clamping corneas at the scleral rim can create artificial boundary conditions that can potentially affect corneal birefringence, the clamping geometry of the artificial chamber in our phantom minimized the stress on the sclera.³⁸

The results of our polarimetric approach for determining glucose concentration inside the corneas clamped on an artificial anterior chamber are presented in Figs. 7 and 8. Similar to the *in vitro* observations, a single-wavelength system using either wavelength is unable to predict the glucose concentration *ex vivo* with precision. The mean standard error of prediction was calculated as 125.4 and 151.1 mg/dL for the individual wavelengths of 635 nm and 532 nm, respectively. These results again highlight the problem of corneal birefringence masking the signal due to the optical activity of glucose. However, when the information from both wavelengths is combined and analyzed using MLR, the error in estimation is reduced significantly to a mean value of 22.4 mg/dL and appeared much more linear, with a correlation coefficient of 0.996. This further demonstrates the potential of the dual-wavelength approach to compensate for the time-varying corneal birefringence.

It was noted that the noise in the measurement signal was slightly more pronounced in the case of *ex vivo* cornea experiments compared to *in vitro* plastic phantom experiments, and is evident by the sensitivity of the system in the respective experiments. We believe that one of the major factors contributing to this relative reduction in accuracy is the corneal tissue compliance. Although the clamping of the cornea approximates the

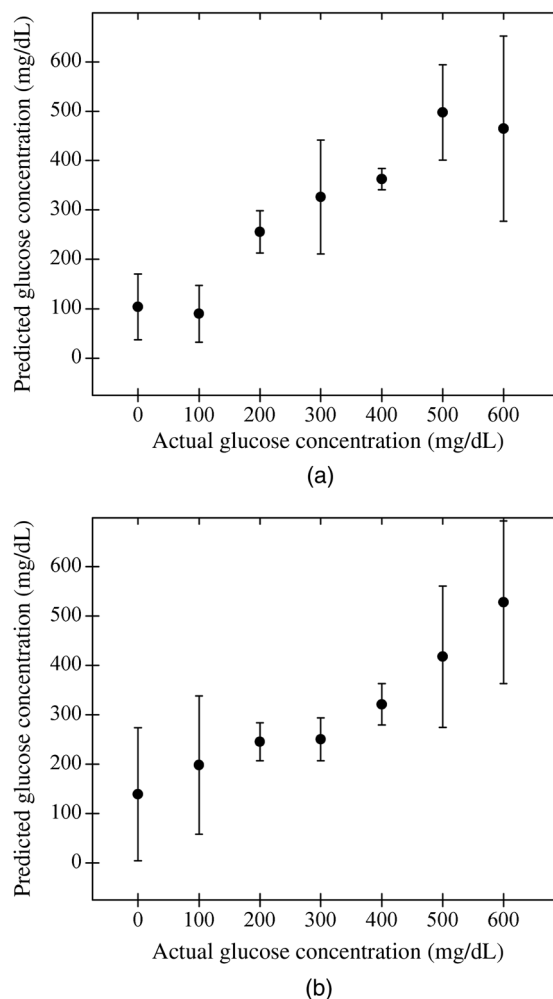


Fig. 7 Mean estimated glucose concentration as a function of actual glucose concentration for the *ex vivo*, single-wavelength model using (a) 635-nm and (b) 532-nm wavelengths. Note that the error bars represent the variation between three separate experiments and are large, showing the inability of a single-wavelength model to predict glucose concentration.

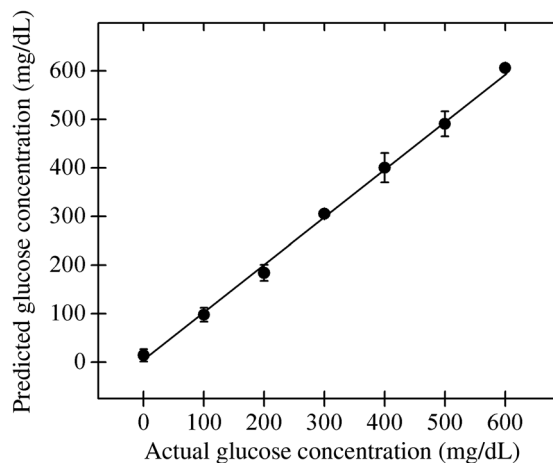


Fig. 8 Mean estimated glucose concentration as a function of actual glucose concentration for the *ex vivo*, dual-wavelength model. The error bars represent the variations among three separate experiments and are reduced significantly relative to the single-wavelength models.

in vivo environment, changing the glucose concentration in the artificial anterior chamber results in a pressure cycle. This behavior was previously studied in detail by Boyce et al.³⁹ In their constrained inflation experiments, it was observed that the viscoelastic behavior of the cornea generated hysteresis in the pressure-deformation response at the apical region. Moreover, mechanical behavior such as creep and relaxation was also noticed for a constant inflation pressure and a constant inflation volume, respectively. Such hysteresis and biomechanical response can physically move the region on the cornea being probed by the laser beam, during and in between measurements, resulting in a long-term drift in the polarimetric signal. We quantified this sample noise by determining the variation within and across signal measurements. As mentioned above, each measurement is based on a 10-point running average. The standard deviation within these 10 points in a single measurement, in terms of glucose concentration, was found to be similar (~6 mg/dL) for both *in vitro* plastic phantom and *ex vivo* cornea phantom measurements. Because the PID was running much faster than the induced motion, a 10-point moving average was used in order to better ensure that the value recorded is characteristic of several points at that given time, rather than a single-point measurement. In contrast, the standard deviation of 10 disparate measurements taken at one-minute time intervals was relatively higher for *ex vivo* cornea phantom measurements (~65 mg/dL) when compared to that for *in vitro* plastic phantom measurements (~17 mg/dL). This corneal hysteresis type of response in the *ex vivo* cornea phantom experiments represents an artificial added noise source and the biomechanical response *in vivo* will clearly be much less pronounced since the intraocular pressure variation is controlled physiologically and is limited to a much smaller range in normal eyes.

5 Conclusion

In summary, we have presented a dual-wavelength optical polarimeter for glucose sensing using two unique phantoms: (1) an *in vitro*, custom-built plastic ocular phantom; and (2) an *ex vivo* phantom using pressurized excised New Zealand White rabbits' corneas mounted on an artificial eye anterior chamber. The results demonstrate that compensating for the change in birefringence induced with motion for a limited range on the order of what has been reported *in vivo* in humans, when the system is appropriately aligned, allows for successful detection of glucose concentration.³³ Although the *ex vivo* experiments were subject to slightly higher sample noise, we concluded that this was due to hysteresis in the signal because of the biomechanical pressure changes introduced by the collapse and inflation of the cornea when changing the glucose concentration. The results are encouraging, and future work will focus on creating a slightly faster feedback algorithm for *in vivo* studies in order to compensate for potential saccadic eye movements, which occur at a rate that is an order of magnitude faster than the motion artifacts due to the respiratory and the cardiac cycles.

Acknowledgments

This work was supported by the National Institutes of Health under Grant R01DK076772. The authors would like to thank Dr. Vincent Gresham, clinical veterinarian at the Comparative Medicine Program at Texas A&M University, for harvesting rabbits' eyes and for helpful discussions.

References

1. B. H. Malik and G. L. Cote, "Real-time, closed-loop dual-wavelength optical polarimetry for glucose monitoring," *J. Biomed. Opt.* **15**(1), 017002 (2010).
2. K. C. Hadley and I. A. Vitkin, "Optical rotation and linear and circular depolarization rates in diffusively scattered light from chiral, racemic, and achiral turbid media," *J. Biomed. Opt.* **7**(3), 291–299 (2002).
3. B. D. Cameron, "The application of polarized light to biomedical diagnostics and monitoring," Ph.D. Thesis, Texas A&M University, College Station, Texas (2000).
4. D. J. Donohue et al., "Numerical modeling of the cornea's lamellar structure and birefringence properties," *J. Opt. Soc. Am. A* **12**(7), 1425–1438 (1995).
5. T. Nishida, "Cornea," in *Cornea*, J. H. Krachmer, M. J. Mannis, and E. J. Holland, Eds., 2nd ed., Elsevier-Mosby, Philadelphia, Pennsylvania, Vol. 1 (2005).
6. H. F. Edelhauser, "The balance between corneal transparency and edema: the proctor lecture," *Invest. Ophthalmol. Vis. Sci.* **47**(5), 1755–1767 (2006).
7. G. J. Van Blokland and S. C. Verhelst, "Corneal polarization in the living human eye explained with a biaxial model," *J. Opt. Soc. Am. A* **4**(1), 82–90 (1987).
8. R. Knighton, X.-R. Huang, and L. A. Cavuoto, "Corneal birefringence mapped by scanning laser polarimetry," *Opt. Express* **16**(18), 13738–13751 (2008).
9. B. H. Malik and G. L. Cote, "Modeling the corneal birefringence of the eye toward the development of a polarimetric glucose sensor," *J. Biomed. Opt.* **15**(3), 037012 (2010).
10. E. Hecht, *Optics*, 4th ed., Addison Wesley, San Francisco (2001).
11. R. A. Farrell, D. Rouseff, and R. L. McCally, "Propagation of polarized light through two- and three-layer anisotropic stacks," *J. Opt. Soc. Am. A* **22**(9), 1981–1992 (2005).
12. M. Born and E. Wolf, *Principles of Optics*, Cambridge University Press, New York (1998).
13. D. J. Donohue et al., "A numerical test of the normal incidence uniaxial model of corneal birefringence," *Cornea* **15**(3), 278–285 (1996).
14. R. W. Knighton and X. R. Huang, "Linear birefringence of the central human cornea," *Invest. Ophthalmol. Vis. Sci.* **43**(1), 82–86 (2002).
15. W. A. Christens-Barry et al., "Spatial mapping of polarized light transmission in the central rabbit cornea," *Exp. Eye Res.* **62**(6), 651–662 (1996).
16. M. G. Ducros et al., "Polarization sensitive optical coherence tomography of the rabbit eye," *IEEE J. Sel. Top. Quantum Electron.* **5**(4), 1159–1167 (1999).
17. R. H. Andreo and R. A. Farrell, "Corneal small-angle light-scattering theory: wavy fibril models," *J. Opt. Soc. Am.* **72**(11), 1479–1492 (1982).
18. E. P. Chang, D. A. Keedy, and J. C. Chien, "Ultrastructures of rabbit corneal stroma: mapping of optical and morphological anisotropies," *Biochim. Biophys. Acta* **343**(3), 615–626 (1974).
19. B. H. Malik and G. L. Coté, "Characterizing dual wavelength polarimetry through the eye for monitoring glucose," *Biomed. Opt. Express* **1**(5), 1247–1258 (2010).
20. B. D. Cameron and H. Anumula, "Development of a real-time corneal birefringence compensated glucose sensing polarimeter," *Diabetes Technol. Ther.* **8**(2), 156–164 (2006).
21. Q. Wan, G. L. Cote, and J. B. Dixon, "Dual-wavelength polarimetry for monitoring glucose in the presence of varying birefringence," *J. Biomed. Opt.* **10**(2), 024029 (2005).
22. R. Rawer, W. Stork, and C. F. Kreiner, "Non-invasive polarimetric measurement of glucose concentration in the anterior chamber of the eye," *Graefes Arch. Clin. Exp. Ophthalmol.* **242**(12), 1017–1023 (2004).
23. R. R. Ansari, S. Bockle, and L. Rovati, "New optical scheme for a polarimetric-based glucose sensor," *J. Biomed. Opt.* **9**(1), 103–115 (2004).
24. G. Purvinis, B. D. Cameron, and D. M. Altrogge, "Noninvasive polarimetric-based glucose monitoring: an *in vivo* study," *J. Diabetes Sci. Technol.* **5**(2), 380–387 (2011).
25. M. J. Goetz, Jr., "Microdegree polarimetry for glucose detection," Masters Thesis, University of Connecticut, Storrs, Connecticut (1992).

26. A. M. Winkler, G. T. Bonnema, and J. K. Barton, "Optical polarimetry for noninvasive glucose sensing enabled by Sagnac interferometry," *Appl. Opt.* **50**(17), 2719–2731 (2011).
27. S. N. Savenkov et al., "Generalized matrix equivalence theorem for polarization theory," *Phys. Rev. E* **74**(5), 056607 (2006).
28. S. C. Chapra and R. P. Canale, *Numerical Methods for Engineers*, 2nd ed., McGraw-Hill, New York (1988).
29. R. Knighton, "Spectral dependence of corneal birefringence at visible wavelengths," *Invest. Ophthalmol. Vis. Sci.* **43**, 152 (2002).
30. K. Irsch et al., "Modeling and minimizing interference from corneal birefringence in retinal birefringence scanning for foveal fixation detection," *Biomed. Opt. Express* **2**(7), 1955–1968 (2011).
31. M. Montagnana et al., "Overview on self-monitoring of blood glucose," *Clin. Chim. Acta* **402**(1), 7–13 (2009).
32. D. D. Cunningham and J. A. Stenken, *In Vivo Glucose Sensing*, Wiley, Hoboken, New Jersey (2009).
33. M. A. Kowalska, H. T. Kasprzak, and D. Robert Iskander, "Comparison of high-speed videokeratometry and ultrasound distance sensing for measuring the longitudinal corneal apex movements," *Ophthalm. Physiol. Opt.* **29**(3), 227–234 (2009).
34. J. S. Baba et al., "Effect of temperature, pH, and corneal birefringence on polarimetric glucose monitoring in the eye," *J. Biomed. Opt.* **7**(3), 321–328 (2002).
35. H. Ohkita et al., "Birefringence reduction method for optical polymers by the orientation-inhibition effect of silica particles," *Appl. Phys. Lett.* **84**(18), 3534–3536 (2004).
36. A. Gwon, "The rabbit in cataract/IOL surgery," in *Animal Models in Eye Research* P. A. Tsonis, Ed., Academic Press, Philadelphia, Pennsylvania (2008).
37. Z. Xiao, C. Wang, and Y. Hao, "The *in vitro* study of pressure change effect on corneal birefringence," *Ophthalm. Res* **43**(3), 159–68 (2010).
38. S. Hodson et al., "Observations on the human cornea *in vitro*," *Exp. Eye Res.* **32**(3), 353–360 (1981).
39. B. L. Boyce et al., "Full-field deformation of bovine cornea under constrained inflation conditions," *Biomaterials* **29**(28), 3896–3904 (2008).